Int. J. Electrochem. Sci., 9 **(2014)** 5763 - 5775

International Journal of
ELECTROCHEMICAL
SCIENCE
www.electrochemsci.org

Electrodeposited Pt and PtRu Nanoparticles without Hydrogen Evolution Reaction on Mesoporous Carbon for Methanol Oxidation

Huei-Yu Chou[*], *Tsung-Kuang Yeh and Chuen-Horng Tsai*

Department of Engineering and System Science, National Tsing Hua University, Hsinchu 30013, Taiwan
[*]E-mail: herman7116@gmail.com

Received: 26 May 2014 / *Accepted:* 29 June 2014 / *Published:* 16 July 2014

Platinum nanoparticles (Pt NPs) and Platinum-Ruthenium nanoparticles (PtRu NPs) were pulse-electrodeposited (pulse-ECD) on porous carbon (PC). The applied potentials for pulse-ECD were controlled either in the hydrogen evolution reaction (HER) potential range or not. The size of Pt NPs and PtRu NPs prepared via pulse-ECD with HER potential range are 19.45 nm and 5.86 nm, respectively. In comparison with the size of Pt NPs and PtRu NPs prepared via pulse-ECD within nonHER potential range are 19.45 nm and 6.56 nm respectivtly. The efficiency of the electrocatalyst on methanol oxidation is in terms of electrochemical mass activity (ECMA, normalized current density of methanol oxidation per gram of catalyst loading). The ECMA of the commercial Pt nanocatalysts, our prepared Pt NPs and PtRu NPs using pulse-ECD within HER potential ranges were 78 Ag^{-1}_{Pt}, 957.56 Ag^{-1}_{Pt}, 1013.43 Ag^{-1}_{Pt}, respectively. The ECMA of the commercial PtRu nanocatalysts, our prepared Pt NPs and PtRu NPs using pulse-ECD within nonHER potential ranges were 141 Ag^{-1}_{Pt}, 1274.05 Ag^{-1}_{Pt}, 1465.89 Ag^{-1}_{Pt} respectivtly. TEM diffraction pattern (D.P.) of the nanoparticles deposited within nonHER's potential ranges shown that the highly distortion in the crystal lattice. The results of TEM D.P. characterized that the nonHER's pulse-ECD enhanced the interfacial bonding between the carbon surface and nanoparticles. It is proved that the electrodepostion Pt NPs and PtRu NPs which applied nonHER potential ranges will increase the performance of methanol oxidation.

Keywords: Pt, PtRu, nanoparticles, hydrogen evolution reaction, methanol oxidation

1. INTRODUCTION

Promoting energy demands, depletion of fossil fuel reserves, and environmental pollution have accelerated the search for energy conversion devices with high efficiency and low emissions. One of the most prospective power sources for easy and convenient applications is the direct methanol fuel

cell (DMFC) due to its simple handling and processing of fuel. Because of its easy handling and portable applications, DMFC based on a polymer electrolyte membrane became attractive. Nevertheless, several problems impede their practical uses. Developing more active catalysts for methanol oxidation, reducing the loading of nobel catalysts and improving their effectiveness is critical to the effort of this study.[1-3] Conventional processing for prepared nanocatalysts are well exploited by the methods of impregnation, colloidal, and microemulsion those systematically summarized by Hansan Liu etc.[1] In these synthesizing catalyst processes for anode in the direct methanol fuel cell, noble catalyst bonded with electrode using a binder, such as Nafion solution in commercial catalyst, its efficiency of methanol oxidation is not so high because the catalysts isn't in a good adhere to the electrode which result in the electrolyte phase with small pores may not be accessible to the ioner or methanol, and induces tremendous heterogeneous interface between bonding media and catalysts. A significant decrease in the diffusion rate of the reactant towards the catalytic sites with a thicker active layer was always resulted. While higher catalyst loading generally comes an agglomeration catalyst on the electrode which increases particle size of the catalyst, thus decreasing their efficiency. Some research in recent years is to develop more precise and novel synthesized Platinum (Pt) or platinum-ruthenium (PtRu) nanoparticle (NPs) such as hydrothermal and solveothermal techniques, sol-gel and electrodeposition.[4-9] According to the merits of electrodeposition in contact electrical resistance with electrode, few topics in our group have been initiated involving electrodeposited catalysts of noble metal by galvanization pulses.[10-12] With these electrodeposition process, it may control catalyst particle in a few nanometers and obtain a better character of a catalyst which is comparison with those catalysts in conventional processing.[13-15] It approved that the Pt or PtRu electrodeposited catalyst for higher contact surface with the carbon nanotube (CNT) electrode is a potential process.[14-16] Those Pt or PtRu catalysts electrodeposition potential are selected within HER range for a rapid process, whose potential is lower than -0.24VSCE. These nanocatalyst reductions from precursor is always companies with tremendous hydrogen gas on the carbon electrode surface or Pt surface, and that brings about a diffusion barrier to partially separate reactant solution, chloroplatinic acid, from carbon electrode or nanocatalyst and to form an unstable porous nanocatalyst on the PC. To our knowledge, it is the lack of relevant detail studies to explore the characters of electrodeposited Pt and PtRu using a potential range without the hydrogen evolution reaction (HER). i.e. Pt and PtRu catalysts reduced on the carbon surface absent of hydrogen production. Theoretically, the catalyst electrodeposited within HER potential ranges on the carbon electrode which interference by hydrogen will produce a rough or accumulative catalyst surface. In case of involving HER, catalysts would induce a number of defects and pores in the catalyst or on the interface of catalyst and electrode which cause a harmful effect such as the self-sintering phenomenon of high electrical resistance. The catalyst sintering in electrochemical process included both lateral agglomeration of the clusters and structural reorganization in the clusters, even if arriving at the surface of the catalyst. The changes in surface area and roughness of Pt NPs during ageing were discussed in terms of thermal sintering processes for supporting catalysts.[16, 17]

Our goal is to approach a high efficiency and stable nanocatalyst using electrodeposition process combined with porous carbon as a supporting material. . A prorous carbon (PC) with a high surface area replace of CNT as an electrode material for supporting catalyst for DMFC is to seek a

higher catalyst dispersion and a larger contact surface and good adhesive between catalyst and PC, which accordingly leads to a distinct increase in the active surface area and/or to a reduction in Pt or PtRu loading.[1, 18-21] Pt and PtRu nanocatalyst synthesized by different electrodeposition conditions were analysized to analysize the mechanism between different catalyst structures and compositions with mass activity in methanol oxidation. With electrochemical analysis, it is to approach a better catalyst electrodeposited within nonHER potential ranges on the carbon electrode, and to evaluate the electrochemical performance, which will clarify the relationship between catalyst and electrode via microstructure analysis.

2. EXPERIMENTAL METHODS

2.1 Preparation of porous carbon

To fabricate PC, a carbon slurry prepared by mixing with highly activated carbon powder (ACP, DARCO-FGD Norit Co.), having initial specific surface area of > 600 m^2/g estimated by Brunauer, Emmett and Teller (BET) theory, was applied to fabricate PC with chop carbon fiber in 10mm length as active carbon powder support (Toray T300-3k), and phenol formaldehyde resin (reagent grade) as a binder. After stirring the mixture with alcohol for 1 h to ensure the homogeneity, it was cast directly in a silicone rubber mold with a thickness of <500 μm using a casting knife. The cast film was subsequently dried in 160 °C for 24 h to keep phenolic resin totally curing. Finally, the cast plate after curing was carbonized in 1400 °C with Argon (Ar) atmosphere for 1 h to carbonize the phenol formaldehyde resin. The weight ratios of carbon slurry, ACP/carbon chops fiber/ phenolic resin /alcohol to be 55/5/15/25, were employed in this study.

2.2 Surface morphology characterization and pore size measurements

To characterize the physical structure of the prepared electrode, the morphologies and structures of the specimens were characterized by scanning electron microscope (*SEM*, JEOL JSM-6330F), High Resolution Transmission Electron Microscopy (HRTEM, JEM-2100F), and energy dispersive spectrometers (EDS, Oxord TEM100). The pore size and pore size distribution of the electrodes were analyzed using an automatic surface area & pore size analyzer (Autosorb-1, Quantachrome instruments). The loadings of Pt and PtRu were estimated by inductively coupled plasma-mass spectrometer (ICP-MS, SCIEX ELAN 5000. Perkin Elmer).

2.3 Characterization of electrochemical properties

With a three-electrode electrochemical cell, Pt and PtRu NPs were electrodeposited onto the foregoing specimens, PC, in a potentiostatic approach in the citric acid (CA) as the aqueous solution. Pt wires served as the counter electrode and a saturated calomel electrode (SCE) were used as the reference electrode. For the electrodeposition of Pt and PtRu, 0.4 mM $H_2PtCl_6 \cdot 6H_2O$ (Alfa Aesar®),

with and without 1.6 mM $RuCl_3 \bullet xH_2O$ (Alfa Aesar®) were formulated in 0.2 M aqueous CA solutions as a precursor.[12, 22] The electrochemical performance of the electrode was evaluated by Cyclic Voltammetry (CV) using a potentiostat (Model CHI-1140B, CHI instruments, Inc). The deposition electrolytes were saturated with an Ar gas during deposition processes conducted under ambient pressure and a controlled temperature of 30 °C and with magnetic stirring. The Pt/PC and Pt-Ru/PC prepared in the aqueous solution at two reduce potential -0.45 (HER potential range) and $-0.24V_{SCE}$ (nonHER potential range) were denoted as H-Pt , H-PtRu and nH-Pt, nH-PtRu , respectively. After the electrodeposition process to accumulated electrocharge with 2 Coulumbs in square centimeters of PC, the catalytic electrodes (H-Pt, H-PtRu and the nH-Pt, nH-PtRu) were thoroughly cleansed with distilled water. The apparent area of PC electrode was 1x1 cm^2. To compare the effectiveness with each specimen, we normalized the area by Pt loading.[23-25] Before the electrochemical tests in Ar saturated 1 M CH_3OH + 0.5 M H_2SO_4 aqueous solutions, each specimen was activated by CV at a scan rate of 50 mV sec^{-1} with potentials ranging from -0.25 to +1.0 V_{SCE} for 7 cycles in an Ar saturated 0.5 M H_2SO_4 aqueous solution. CV analyses for evaluating the methanol oxidation efficiency of the specimens were conducted at a scan rate of 20 mV sec^{-1} with potentials ranging from -0.2 to +0.85 V_{SCE} for 7 cycles. An CHI-1140B potentiostat was used in all electrochemical operations.[10-12] For the electrodeposition of Pt and PtRu, 0.4 mM $H_2PtCl_6 \bullet 6H_2O$ with and without 0.16 mM $RuCl_3 \bullet xH_2O$ were formulated in aqueous CA solutions as precursors. The deposition electrolytes were saturated with an Ar gas after 30 minutes purging during the deposition processes conducted under ambient pressure and a controlled temperature of 30 °C and with magnetic stirring.

3. RESULTS AND DISCUSSION

3.1 Characterization of the Porous carbon-supported Pt and PtRu

Preparation of PC using phenol formaldehyde resin is similar to Chai, etc.[19, 26] It concluded that the higher temperature heat treatment of PC was improved the effect of catalyst electrodeposition. The PC substrates were heated at 1400 °C with Ar for 1h in this work. PC was later measured the specific surface area and pore size distribution (PSD) by surface area & pore size analyzer, and the results showed in Figure 1. Figure 1 (a) shows the specific surface area of the prepared PC. The cumulative specific surface area of PC is 37.175 m^2g^{-1}. By integrating the curve of specific surface with different pore, the result of different pore volume distribution curve respect to different pore, shown as Figure 1 (b). The specific cumulative pore volume of PC is 0.088 ml g^{-1}. The pore size of the forgoing PC included the activated carbon is probably because the high-temperature heating which drove PC's surface energy to a lower level, and also might much narrow the small pore size even the active carbon with initial specific surface area of > 600 m^2g^{-1}.[27, 28]

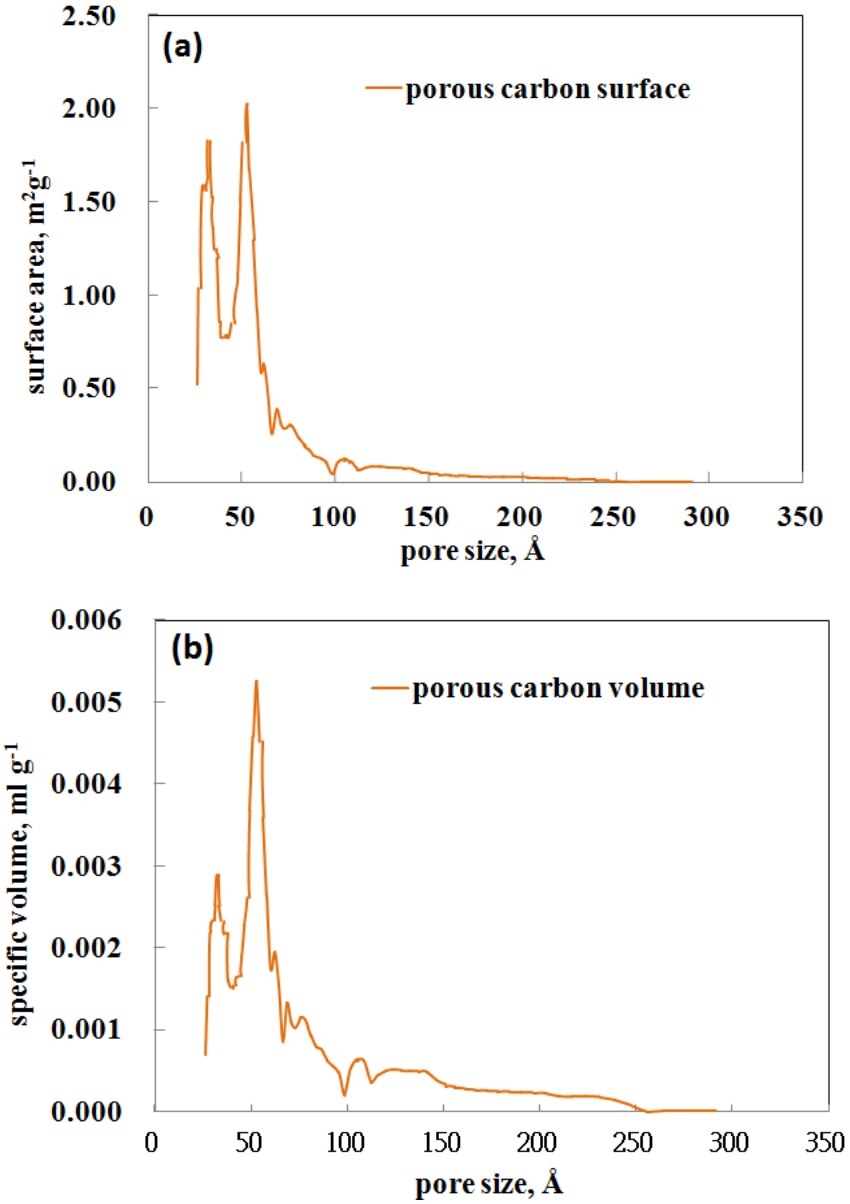

Figure 1. BET measurements of (a)The cumulative specific surface area of PC is 37.175m^2 g^{-1}, (b) The specific cumulative pore volume of PC is 0.088 ml g^{-1}.

The aqueous binder, phenol formaldehyde resin (PF750, CCP), in this high temperature heat-treatment will become porous material which can avoid the pore sealing in the active carbon of PC. On average, the pore size of heated PC is 52.66 Angstrom (Å). A PC as an anode for DMFC is used to control the mass transfer from the methanol reservoir to the anode. Therefore the larger pore size provides more effective for methanol diffused or transported via the pore to the interface between catalyst and Nafion. [15, 19, 21] In this study, the PC was used as a substrate to electrodeposite nanocatalysts in HER potential range (-0.45V_{SCE} HER), and the nonHER potential range (-0.24 V_{SCE}) to investigate the effect of methanol oxidation with the produced hydrogen, and the hydrogen effect for Pt and PtRu nanocatalysts deposition. The morphologies of our prepared nanocatalyst are observed by SEM which shown as Figure 2. Pt NPs were electrodeposited on PC applied the potential within the

HER and nonHER potential ranges, denoted as H-Pt and nH-Pt, shown as Figure 2(a) and (b), respectively. The co-electrodeposited PtRu NPs on PC applied the potential within the HER and nonHER potential ranges, denoted as H-PtRu and nH-PtRu, shown as Figure 2(c) and (d), respectively.

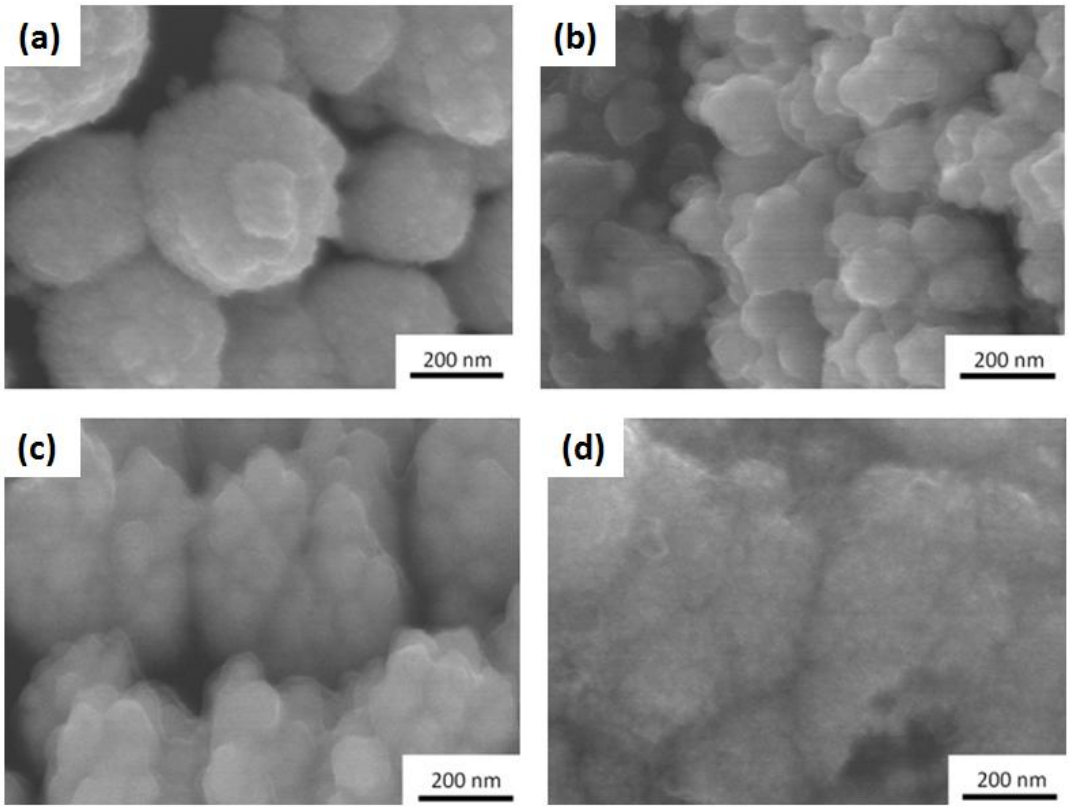

Figure 2. SEM image of of (a) H-Pt, (b) nH-Pt, (c) H-PtRu, and (d) nH-PtRu, respectively.

From SEM images of H-Pt or nH-Pt, the surface appears rough morphologies of irregular surface shape. Compare with Figure 2(a) and (b), it can be observed the agglomeration particle mostly more than 100nm in diameter, which is gathered by a number of nanoparticles. A sharp and deep valley morphology was clearly observed between agglomeration particles. It is inferred that the initial co-electrodepositing hydrogen and nanocatalyst adsorbed on the PC surface. We herein proposes that the subsequent electrodeposition solution cannot transport to PC surface which resulting in a void or deep valley. Theoretically, a new Pt crystal after nucleation and growth on PC surface becomes a new electronic conductive path in next electrodeposition pulse, it also can to have a new active site on the Pt surface by hydrogen ion reduced to hydrogen gas. That would make the Pt nanocatalyst surface more porous and rough as the hydrogen evolution rate is higher. The same observation is similar to other metal electrodeposition because HER is a common phenomenon of plating.[13, 14, 29] In the same condition of HER for PtRu electrodepoited on PC, it has found the same deep valley phenomenon in Figure 2(c) as those of Figure 2(a). These valley morphology is caused by hydrogen production. Compared the morphology of Figure 2 (c) with (d) electrodeposited PtRu nanocatalyst, their surface is smoother than those of Pt. This is because the Pt and PtRu nanocatalyst are

simultaneously co-electrodeposited on PC. We postulated that the Pt and Ru electrodeposition in negative potential exhaust plating concentration near the PC surface, followed by a potential of the diffusion potential range (+0.5 V_{SCE}) to recover plating concentration near the PC surface. Part of electrodeposited Ru on nanocatalyst surface will immediately and homogeneously recombine with OH^- from water to randomly form a soluble RuOH.[30, 31] Therefore, the nanocatalyst surface is unlike H-Pt or nH-Pt with a rough surface morphology. Instead, a smooth surface of these PtRu can be identified in Figure 2 (c) and (d).

3.2 Methanol oxidation of Pt and PtRu supported on the porous carbon

Figure 3 is the CV measurements of the Pt and PtRu electrodeposited on PC (1cm * 1cm) in the solution (1M CH_3OH + 0.5M H_2SO_4 in DI water), and normalized by a Pt loading amount from ICP-MS analysis of mass activity. The electrochemical characteristics of CV results are summarized in Table I including Pt/Ru molar ratio, i_f/i_b ratio, peak potential (V_{SCE}), and mass activity ($Ag^{-1}{}_{Pt}$).

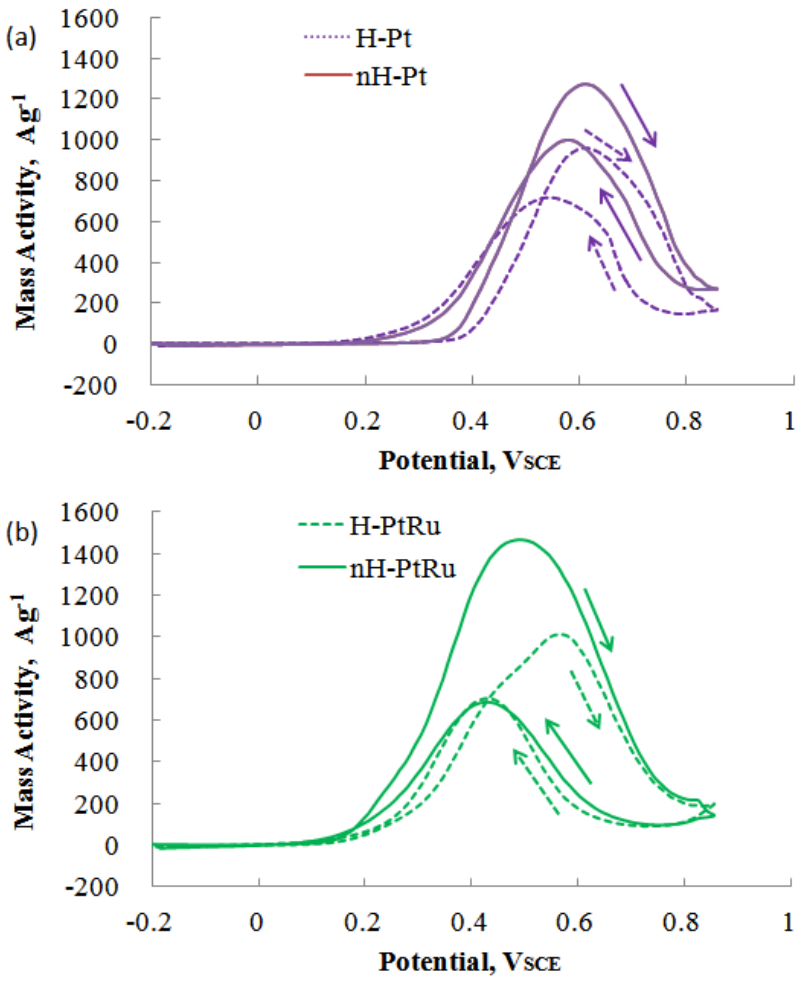

Figure 3. CV measurements in 1M CH_3OH and 0.5M H_2SO_4 solution and normalized by Pt loading. (a) H-Pt and nH-Pt, and (b) H-PtRu and nH-PtRu.

Report to our previous results, the mass activity of H-Pt is 2.658 times of Pt/CNT's, is 10 times more than the commercial catalyst (E-Tek, Pt/C) shown as Table 1. This should be accessible explaining the difference between the PC and CNT, the pore of PC can assist the methanol diffusion to the position of nanocatalyst, also may release and emit CO_2 by pore after methanol oxidation.

Table 1. Summary of electrochemical characters of CV analysis from Figure 2.

Samples	Loading Pt/Ru (μgcm^{-2}) By ICP-MS	Pt/Ru Molar ratio	Vp (V_{SCE})	i_f/i_b	Max. Mass activity (Ag^{-1}_{Pt})	Mass activity at 0.4V_{SCE} (Ag^{-1}_{Pt})
H-Pt	33.6	100/0	0.61	1.34	957.56	116.98
nH-Pt	123.7	100/0	0.61	1.27	1274.05	273.57
H-PtRu	61.2/14.73	68.28/31.72	0.57	1.44	1013.43	640.49
nH-PtRu	131.9/25.53	72.81/27.19	0.50	2.13	1465.89	1289.13
E-Tek Pt/C[1])	-	100/0	-	1.23	78	-
E-Tek PtRu/C[19])	-	50/50	-	-	141	46
Pt/CNT [10])	402.2	100/0	0.62	1.02	360.5	24.86
PtRu/CNT[12])	274.5/70.4	66.79/33.21	0.505	2.94	1038.3	811.2
Pt/mesoporous[1])	-	100/0	0.75	-	215	-

Even if nanocatalyst spreading in a large contact area does not affect the CO_2 emissions from catalyst or methanol diffusion. Similarly, the specimen of H-PtRu have a high mass activity the same as that of the CNT. Compared the mass activity of Pt with that of PtRu, PtRu mass activity has a higher mass activity due to PtRu alloy after electrodeposition formed the RuOH with water which having synergy effect with Pt nanocatalyst for methanol oxidation.[32] Long et al mentioned that alloyed PtRu does not improve the activity, but PtRuOxHy can promote it.[31] Because the Ru transformed to RuOH with H2O can capture CO from the adjacent PtCO and reduced Pt. The CO_2, release gas, is from RuOH with CO. Ru in PtRu alloy with water can also be easily changed into RuOH in reduction potential.[2, 30, 31]

Compared PtRu nanoparticle to the solid-solution PtRu grain, the solid-solution alloyed PtRu prohibits the diffusion of water or methanol into the catalyst. Instead, H_2O and methanol are easily diffused into the Pt and PtRu nanoparticles. It will result in Pt fully utilized by the synergy effect of RuOH.[2, 31] It can explain that PC surface is not dominated for mass activity, but Ru exist in Pt crystal structure. The mass activity of nH-Pt is 1.33 times that of H-Pt. The anodic peak potential (Vp) in this study is in the range of 0.61V_{SCE} which is referring to the peak potential of 0.6V_{SCE} from several studies. [10,20,37,38] Theoretically, we know that peak potential strongly depends on the Pt surface which partially covered by the CO or Pt oxide caused by the methanol oxidation reaction. More oxidation reactions shift the peak potential more positive. That is because the diffusion barrier such as CO or Pt oxide on the catalyst surface will retard the methanol diffused to the site of Pt catalyst. A similar previous report featured that the energy is needed for ions or methanol molecule to transport in the barrier. [41] Therefore, we suggested that methanol and its intermediates diffused through the barrier need more

energy to overcome the barrier, which resulted in a phenomenon of the positive shift in the peak potential. On the other hand, some content of Ru induced to Pt act as synergizer which will firstly react with water to form RuOH. Secondly, RuOH donated OH to the neighboring Pt atoms to enhance CO oxidation which will remove CO on the Pt surface and make the peak potential negative shift. [37,42] But the size of the nanoparticle is different between nH-Pt and H-Pt, the nanoparticle size of H-Pt is about 2.3nm ~ 16.16nm with an average of 8.19 nm, the size of nH-Pt is about 3.2 nm ~ 35.62 nm with an average particle size of 19.45nm. It can be recognized that the contact area of nH-Pt would be larger than those of H-Pt in the same Pt loading amount. It meant that, from the contact resistance of nanocatalyst, the contact resistance of nH-Pt is obviously less than that of H-Pt. Compare H-PtRu with NH-PtRu, the mass activity of NH-PtRu is 1.44 times that of H-PtRu. But the size of H-PtRu nanoparticle is slightly different with nH-PtRu. The size of H-PtRu nanoparticle is about 1.87 nm ~ 14.42 nm with an average of 5.86 nm, and the size of nH-PtRu nanoparticle is about 2.00 nm~12.92 nm with an average particle size of 6.56 nm. This is because that the Ru reduction amount in PtRu alloy at low temperature is quite low.[31, 33] Most of Ru atoms exist in amorphous or in RuOH after reacting with H_2O rather than in PtRu alloy. Therefore, whether in the HER or nonHER potential ranges, the mass activity is above 1000 Ag^{-1}_{Pt}. From peak potential Vp of forward scanning, the peak potential of H-PtRu is 0.57 VSCE, and that of nH-PtRu is 0.5 VSCE. We herein suggest that this is because electrodeposition current of H-PtRu is higher than that of nH-PtRu which induces electrochemically aging or sintering. The aging phenomenon induced by a high current density with hydrogen evolution in electrodeposition is the same as thermal sintering.[16, 17] Based on the thermal sintering, it will make nanocatalyst reacted with H_2O to form PtO and PtOH in electrodeposition process which would degrade Pt catalytic performance of methanol oxidation and cause a large overpotential.[15, 17, 29] The comparison of the Pt loading of H-Pt/nH-Pt and H-PtRu/nH-PtRu on the PC substrate, the amount of the electrodeposition in HER potential range are less than those of Pt and PtRu within nonHER potential range.

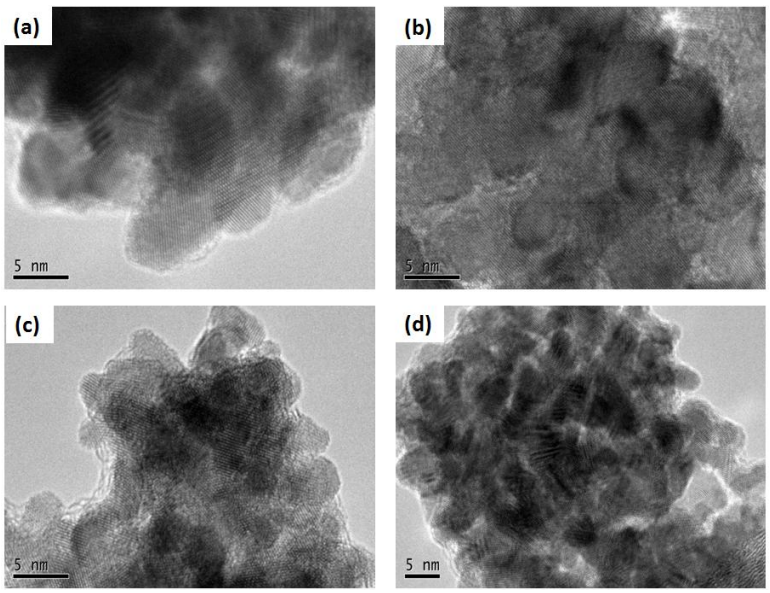

Figure 4. TEM images of (a) H-Pt, (b) nH-Pt, (c) H-PtRu ,and (d) nH-PtRu, respectively.

It is because that the electrodeposition with HER contains nonFaradaic current and the hydrogen production, it consumed the electric energy which invalid for electrodeposition of Pt and PtRu.[14, 31] From Table 1, the Pt/Ru molar ratio of H-PtRu is resembling that of PtRu/CNT. But compared to the Pt/Ru molar ratio of H-PtRu with that of nH-PtRu, it indicated that Ru is difficult to alloy in electrodeposition. From some studies, it is revealed that only 10% Ru or lower can be alloyed in PtRu alloy. Excessive Ru excluded alloyed PtRu would exist in a form such as amorphous structure or transformed into RuOH which mixed with PtRu nanocatalyst.[30, 31] For methanol oxidation, Ru atom necessarily adjacent to Pt atom will have a synergy effect of an efficient performance. Therefore, it is consistent with the mass activity of H-PtRu and that of nH-PtRu even if it has a lower Ru content than that of H-PtRu which showed in Table 1.[33] Due to the instability of aging Pt or PtRu nanocatalyst will appear above 0.4 V_{SCE}, we also listed the mass activity at 0.4 V_{SCE} as a standard criterion in Table 1, the conclusion is the same as the previous discussion.[1]

3.2 Microstructure of Pt and PtRu nanocatalyst supported on porous carbon

The HRTEM images of H-Pt, nH-Pt, H-PtRu, and the nH-PtRu are shown in Figure 4 (a), (b), (c), and (d), respectively. From the HRTEM images, we can determine the d-spacing precisely.Theoretically, chemically well bonding of two heterogeneous materials will create distortion of the lattice, it is just so called coherent bonding. From the TEM image of Figure 4, the d-spacing can be estimated of each nanocatatalyst. The Pt lattice constant of the face centered cubic (F.C.C.) crystal structure is 3.92 Å, which can be used to easily calculate the d-spacing in different index hkl crystallographic plane. The comparison of theoretical value in different d-spacing of Pt(hkl) crystallographic plane, that will induce an error value to see the distortions of electrodeposited Pt and PtRu. According to the d-spacing estimation from the TEM images, a summary of d-spacing (Å), the error value (%) and Pt crystallographic plane (Pt(hkl)) was shown in Table 2.

Table 2. Summary of d-spacing (Å), error value (%) and Pt crystallographic plane (Pt(hkl)) from Figure 4.

Sample	d-spacing, Å	Lattice Error, %	Pt(hkl)
H-Pt	2.3066	1.919	111
	2.0837	6.292	200
nH-Pt	2.0833	6.292	200
	2.7778	22.736	111
H-PtRu	2.2332	1.325	111
nH-PtRu	2.3952	5.832	111

In the Figure 4 (a) of H-Pt, it can be observed that the d-spacing is 2.306 Å of Pt(111) and 2.083 Å of Pt(200) respectively. Compared the estimated d-spacing of those of the theoretical Pt(111) and Pt(200), a slight difference between them is easily found. The lattice error is about 1.92% of Pt(111) and 6.29% of Pt(200), respectively. In the Figure 4 (b) of nH-Pt, it can be clearly observed that

the d-spacing is 2.083 Å of Pt (111) and 2.777 Å of Pt (200) mainly, respectively. Compared the estimated d-spacing with those of the theoretical Pt(111) and Pt(200), a large difference between them is easily found. The lattice error is about 6.29% of Pt(111) and 22.73% of Pt(200), respectively.

The similarity of crystallographic plane in H-Pt and nH-Pt in Table 2 appear the same result of Pt(111) and Pt(200). In most studies with nanoparticle or thin layer, Pt crystallographic plane of Pt(111) and PT (200) is dominately found without crystal high index. That is reasonable that the diffraction of crystallographic planes isn't thick enough to intensify the diffraction peak compared to background.[10, 12] But compared the error value of nH-Pt with that of H-Pt, the distortions of lattice electrodeposited in nonHER potential ranges are higher than those in HER. It is suggested that hydrogen gas takes place during the pulse of negative potential would change the microstructure by tiny pore in H-Pt and bring about slightly brittleness.[13, 29] Some studies in metal electrodeposition stated that the structure of the metal in electrodeposition depends on the hydrogen evolution rate.[13, 34]

In the Figure 4 (c) of H-PtRu, it can be clearly observed that the d-spacing is only 2.233 Å of Pt(111). Compared the estimated d-spacing to that of the theoretical Pt(111), a trivial difference between them is easily found. The lattice error is about 1.325% of Pt(111). In the Figure 4 (d) of nH-PtRu, it can be clearly observed that the d-spacing is only 2.395Å of Pt(111). Compared the estimated d-spacing to that of the theoretical Pt(111), a large difference between them is found. The lattice error is about 5.832% of Pt(111).[35, 36] The correlation of crystallographic plane in H-PtRu and nH-PtRu from Table 2 appeared the same result of Pt(111) shown that nanoparticle of Pt crystallographic plane of Pt(111) is found dominantly. Luo et al explained that the Pt(111) palne was preferable, due to a smaller solution-cluster interfacial energy, so it stacking followed Pt(111) plane.[16] Regarding the distortion of the lattice between the Pt or PtRu and PC, we suspect that the coherent bonding of electrodeposited PtRu within nonHER is better than those of HER. Based on the coherent bonding between catalyst and carbon support, we suspect that it might reduce the contact resistance between them. A low resistance bonding would avoid the thermal sintering during the electrochemical reaction with a high current via the coherent bonding. This assumption of high mass activity of CV is highly consistent with the result of the nonHER lattice distortion from TEM image. Additionally, Ru atoms alloyed in Pt alloy either in H-PtRu or in nH-PtRu is just 27-31atm% shown as Table 1. Some studies stated that only 4-10 atom% Ru is alloyed in PtRu alloy which companioning with the excessive Ru atoms presented in an amorphous structure or RuOH.[2, 30, 31] This result of PtRu identified by TEM and EDS is highly consistent with the ICP-MS's measurement shown as Table 1.

4. CONCLUSIONS

In this work, Pt and PtRu NPs were directly deposited on PC by the Pulse-ECD method at room temperature. The PC with average pore size of 52.66 Å as supporting material is not only providing the pore channel to transport methanol into the interface of the catalyst with carbon, but also offers reaction gases to exit out. Because of no hydrogen generation at nonHER potential ranges, the ECMA of Pulse-ECD Pt NPs and PtRu NPs show great performance by applied nonHER potential. The ECMA of Pt NPs/PC deposited within nonHER potential range is 1274.05 Ag^{-1}_{Pt}, which is 16.33

times compared with the commercial Pt/C. The ECMA of PtRu NPs/PC deposited within nonHER potential range is 1465.89 Ag^{-1}_{Pt}, which is 10.46 times compared with the commercial PtRu/C. We demonstrated that the Pulse-ECD is a potential technique for the preparation of nanocatalyst for methanol oxidation application.

ACKNOWLEDGEMENTS
The authors would acknowledge the financial support from the National Science Council of Taiwan under grant numbers NSC 101-2221-E-007 -047 -MY3.

References

1. H.S. Liu, C.J. Song, L. Zhang, J.J. Zhang, H.J. Wang, D.P. Wilkinson, *Journal of Power Sources*, 155 (2006) 95
2. J.N. Tiwari, R.N. Tiwari, G. Singh, K.S. Kim, *Nano Energy*, 2 (2013) 553
3. S. Wasmus, A. Kuver, *Journal of Electroanalytical Chemistry*, 461 (1999) 14
4. A. Chen, P. Holt-Hindle, *Chem Rev*, 110 (2010) 3767
5. J.Y. Oh, S.H. Jee, N. Kakati, S.H. Kim, M.J. Song, Y.S. Yoon, *Japanese Journal of Applied Physics*, 49 (2010) 115101
6. J.Y. Oh, S.H. Jee, N. Kakati, S.H. Kim, M.J. Song, Y.S. Yoon, *Japanese Journal of Applied Physics*, 51 (2012) 119202
7. S.H. Lee, D.J. Kim, Y.S. Yoon, *Japanese Journal of Applied Physics*, 52 (2013) 035001
8. T. Spataru, P. Osiceanu, M. Marcu, C. Lete, C. Munteanu, N. Spataru, *Japanese Journal of Applied Physics*, 51 (2012) 090119
9. C.F. Tsai, P.W. Wu, P. Lin, C.G. Chao, K.Y. Yeh, *Japanese Journal of Applied Physics*, 47 (2008) 5755
10. M.C. Tsai, T.K. Yeh, C.H. Tsai, *Electrochemistry Communications*, 8 (2006) 1445
11. M.-C. Tsai, T.-K. Yeh, C.-H. Tsai, *Materials Chemistry and Physics*, 109 (2008) 422
12. M.C. Tsai, T.K. Yeh, C.H. Tsai, *International Journal of Hydrogen Energy*, 36 (2011) 8261
13. Z.W. Liu, M. Zheng, R.D. Hilty, A.C. West, *Journal of the Electrochemical Society*, 157 (2010) D411
14. C. Coutanceau, A.F. Rakotondrainibe, A. Lima, E. Garnier, S. Pronier, J.M. Leger, C. Lamy, *Journal of Applied Electrochemistry*, 34 (2004) 61
15. E.A. Franceschini, M.M. Bruno, F.J. Williams, F.A. Viva, H.R. Corti, *ACS applied materials & interfaces*, 5 (2013) 10437
16. M.F. Luo, W.R. Lin, W.H. Wen, B.W. Chang, *Surface Science*, 602 (2008) 3258
17. S.N. Pron'kin, O.A. Petrii, G.A. Tsirlina, D.J. Schiffrin, *Journal of Electroanalytical Chemistry*, 480 (2000) 112
18. G.G. Park, T.H. Yang, Y.G. Yoon, W.Y. Lee, C.S. Kim, *International Journal of Hydrogen Energy*, 28 (2003) 645
19. G.S. Chai, S.B. Yoon, J.S. Yu, J.H. Choi, Y.E. Sung, *Journal of Physical Chemistry B*, 108 (2004) 7074
20. S.H. Liu, W.Y. Yu, C.H. Chen, A.Y. Lo, B.J. Hwang, S.H. Chien, S.B. Liu, *Chemistry of Materials*, 20 (2008) 1622
21. F.Y. Xie, H. Meng, P.K. Shen, *Electrochimica Acta*, 53 (2008) 5039
22. J.W. Guo, T.S. Zhao, J. Prabhuram, C.W. Wong, *Electrochimica Acta*, 50 (2005) 1973
23. L.A. Estudillo-Wong, E.M. Arce-Estrada, N. Alonso-Vante, A. Manzo-Robledo, *Catalysis Today, 166* (2011) 201
24. D.Z. Mezalira, M. Bron, *Journal of Power Sources*, 231 (2013) 113

25. W. Li, A.M. Lane, Electrochemistry Communications, 13 (2011) 913
26. M.J. Watt-Smith, S.P. Rigby, T.R. Ralph, F.C. Walsh, *Journal of Power Sources*, 184 (2008) 29
27. M. Seredych, M. Koscinski, M. Sliwinska-Bartkowiak, T.J. Bandosz, *Journal of Power Sources*, 220 (2012) 243
28. T.X. Nguyen, S.K. Bhatia, *Carbon*, 44 (2006) 646
29. D.R. Gabe, J*ournal of Applied Electrochemistry*, 27 (1997) 908
30. S.R. Brankovic, J.X. Wang, Y. Zhu, R. Sabatini, J. McBreen, R.R. Adzic, *Journal of Electroanalytical Chemistry*, 524 (2002) 231
31. J.W. Long, R.M. Stroud, K.E. Swider-Lyons, D.R. Rolison, *Journal of Physical Chemistry B*, 104 (2000) 9772
32. T.T. Cheng, E.L. Gyenge, *Journal of the Electrochemical Society*, 155 (2008) B819
33. E. Antolini, F. Cardellini, *Journal of Alloys and Compounds*, 315 (2001) 118
34. P.C. Hsu, S.K. Seol, T.N. Lo, C.J. Liu, C.L. Wang, C.S. Lin, Y. Hwu, C.H. Chen, L.W. Chang, J.H. Je, G. Margaritondo, *Journal of the Electrochemical Society*, 155 (2008) D400
35. H.N. Dinh, X.M. Ren, F.H. Garzon, P. Zelenay, S. Gottesfeld, *Journal of Electroanalytical Chemistry*, 491 (2000) 222
36. S.A. Lee, K.W. Park, J.H. Choi, B.K. Kwon, Y.E. Sung, *Journal of the Electrochemical Society*, 149 (2002) A1299
37. Z.B. He, J.H. Chen, D.Y. Liu, H.H. Zhou, Y.F Kuang, *Diamond & Related Materials*, 13 (2004) 1764
38. Y. Chen, G.J. Zhang, J. Ma, Y.M. Zhou, Y.W Tang, T.H. Lu, *international journal of hydrogen energy*, 35 (2010) 10109
39. F. Scholz, R. Gulaboski, K. Caban, *Electrochemistry Communications*, 5 (2003) 929
40. N. Wakabayashi, H. Uchida, and M. Watanabe, *Electrochemical and Solid-State Letters*, 5 - 11 (2002) E62